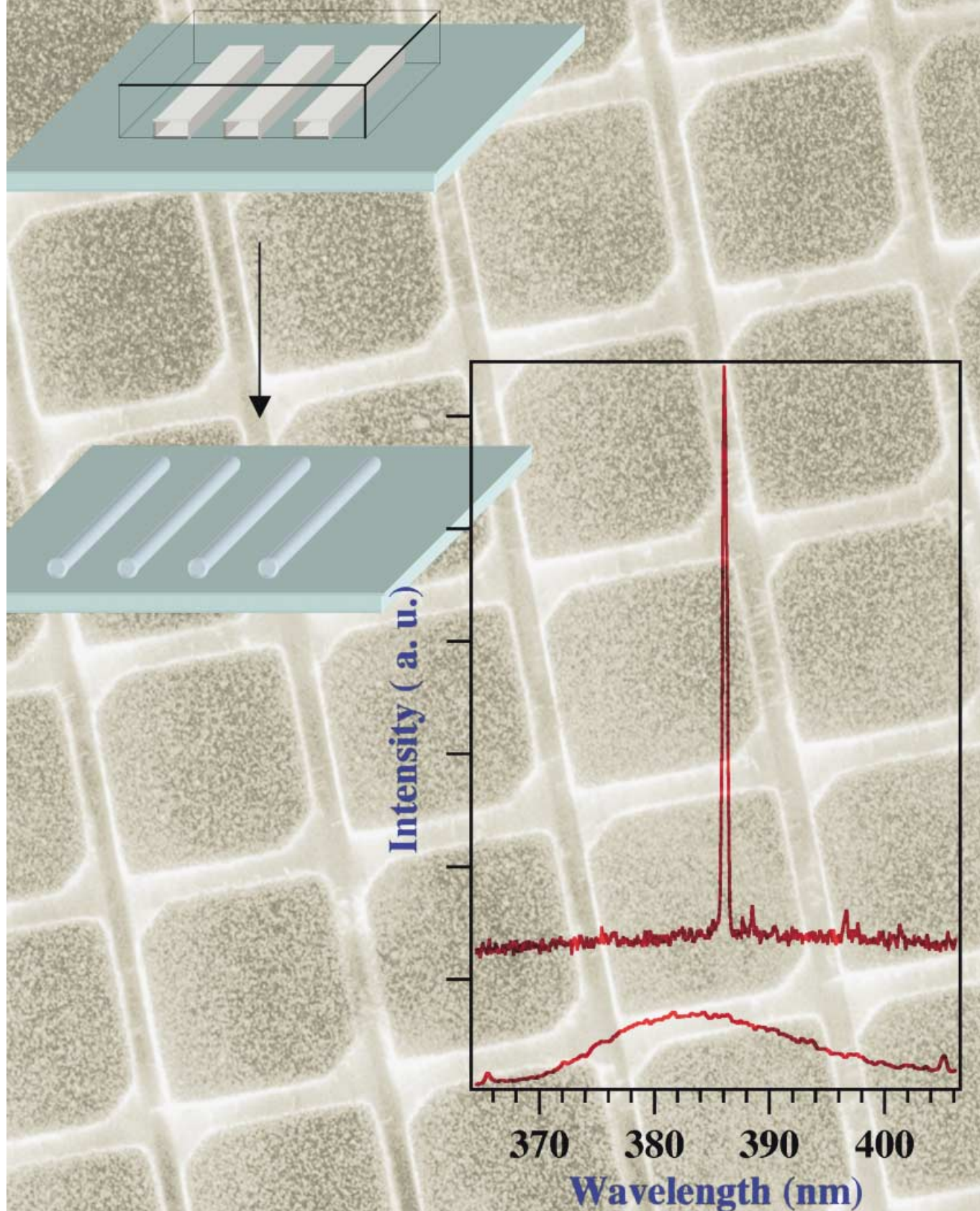


Inorganic Semiconductor Nanowires



Inorganic Semiconductor Nanowires: Rational Growth, Assembly, and Novel Properties

Yiying Wu, Haoquan Yan, Michael Huang, Benjamin Messer,
Jae Hee Song, and Peidong Yang*[a]

Abstract: Rationally controlled growth of inorganic semiconductor nanowires is important for their applications in nanoscale electronics and photonics. In this article, we discuss the rational growth, physical properties, and integration of nanowires based on the results from the authors' laboratory. The composition, diameter, growth position, and orientation of the nanowires are controlled based on the vapor–solid–liquid (VLS) crystal growth mechanism. The thermal stability and optical properties of these semiconductor nanowires are investigated. Particularly, ZnO nanowires with well-defined end surfaces can function as room-temperature ultraviolet nanolasers. In addition, a novel microfluidic-assisted nanowire integration (MANI) process was developed for the hierarchical assembly of nanowire building blocks into functional devices and systems.

Keywords: crystal growth • nanostructures • nanotechnology • nanowires • self-assembly

Introduction

Nanoscale one-dimensional materials have stimulated great interest due to their importance in basic scientific research and potential technology applications.^[1, 2] Many unique and fascinating properties have been proposed and demonstrated for this class of materials, such as metal–insulator transition,^[3] superior mechanic toughness,^[4] higher luminescence efficiency,^[5, 6] enhancement of thermoelectric figure of merit,^[7] and lowered lasing threshold.^[8–10] One-dimensional materials can also be used as building blocks to assemble new generations of nanoscale electronic circuits and photonics.^[11–15]

An important issue in the study and application of one-dimensional materials is how to assemble individual atoms

into one-dimensional nanostructures in an effective and controllable way. A number of nanolithographic techniques, such as electron-beam lithography^[16] and proximal probe patterning,^[17, 18] have been developed. These processes, however, generally are slow and the cost is high. Chemical synthesis represents another important approach to one-dimensional structures.^[19–26] It is much more promising in terms of cost and potential for high volume production. A significant challenge of the chemical synthesis is how to rationally control the nanostructures so that their interfaces and ultimately their two-dimensional and three-dimensional superstructures can be tailor-made towards desired functionality. Below, we present the investigation results from our laboratory directed toward controlled growth of inorganic nanowires. The organization is as follows. In Section 1, we describe the vapor–liquid–solid (VLS) mechanism for nanowire growth used in this study. In Section 2, we introduce a novel vapor–liquid–solid epitaxy (VLSE) process for the controlled nanowire growth. In Sections 3 and 4, we describe the thermal stability and optical properties of these nanowires. In Section 5, a novel microfluidic-assisted nanowire integration (MANI) process will be presented for the purpose of hierarchical assembly of nanowire building blocks into functional devices and systems. Finally, future directions will be discussed.

1. Vapor–Liquid–Solid Nanowire Growth Mechanism

A single-crystalline inorganic nanowire is an interesting example of an anisotropic crystal. The diameter of nanowire is in the range of 1–200 nm and the length is several microns or longer. In general, nanowires are not thermodynamically stable relative to their bulk materials. Consequently, a critical issue in nanowire growth is how to kinetically promote anisotropic crystal growth. A well-accepted mechanism of nanowire growth through a gas-phase reaction is the so-called vapor–liquid–solid (VLS) process proposed by Wagner in 1960s during his studies of large single-crystalline whisker growth.^[27, 28] According to this mechanism, the anisotropic crystal growth is promoted by the presence of liquid alloy/

[a] Prof. P. Yang, Y. Wu, H. Yan, Dr. M. Huang, B. Messer, Dr. J. H. Song
Department of Chemistry
University of California, Berkeley, CA 94720 (USA)
Fax: (+1) 510-642-7301
E-mail: pyang@cchem.berkeley.edu

solid interface. This process is illustrated in Figure 1 for the growth of Si nanowire by using Au clusters as the solvent at high temperature. Based on Si–Au binary phase diagram, Si (from the decomposition of SiH_4 , for example) and Au will form a liquid alloy when the temperature is higher than the eutectic point (363°C , Figure 1 I). The liquid surface has a large accommodation coefficient and is therefore a preferred deposition site for incoming Si vapor. After the liquid alloy becomes supersaturated with Si, Si nanowire growth occurs by precipitation at the solid–liquid interface (Figure 1 II, III).

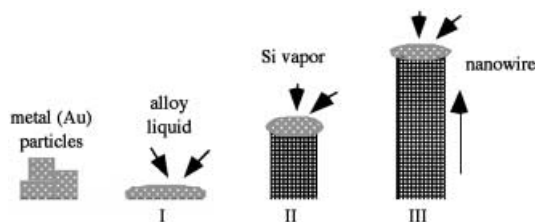


Figure 1. Schematic illustration of vapor–liquid–solid nanowire growth mechanism including three stages: I) alloying, II) nucleation, and III) axial growth.

Recently, real-time observation of Ge nanowire growth was conducted in a high-temperature in situ transmission electron microscope (TEM).^[29] The experiment result clearly shows three growth stages: formation of Au–Ge alloy (Figure 2b, c), nucleation of Ge nanocrystal (Figure 2d) and elongation of Ge nanowire (Figure 2e, f). This experiment unambiguously demonstrates the validity of the VLS mechanism for nanowire growth. The establishment of VLS mechanism at the nanometer scale is very important for the rational control of inorganic nanowires, since it provides the necessary underpinning for the prediction of metal solvents and preparation conditions.

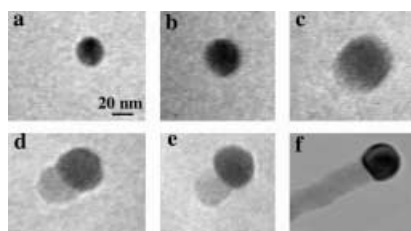


Figure 2. In situ TEM images recorded during the process of nanowire growth. a) Au nanoclusters in solid state at 500°C . b) Alloying is initiated at 800°C , at this stage Au exists mostly in solid state. c) Liquid Au/Ge alloy. d) The nucleation of a Ge nanocrystal on the alloy surface. e) Ge nanocrystal elongates with further Ge condensation, and f) eventually forms a wire.

Based on our mechanism study of the nanowire growth, it is conceivable that one can achieve controlled growth of nanowires at different levels. First of all, one can, in principle, synthesize nanowires of different compositions by choosing suitable solvents and growth temperatures. A good solvent should be able to form a liquid alloy with the desired nanowire material, ideally they should be able to form a eutectic alloy. Meantime, the growth temperature should be set between the eutectic point and the melting point of the nanowire material.

Both physical methods (laser ablation, arc discharge, thermal evaporation) and chemical methods (chemical vapor transport and chemical vapor deposition) can be used to generate the vapor species required during the nanowire growth. As an example, Figure 3 shows Ge nanowires synthesized by a chemical vapor transport process.^[19] Figure 3a shows the

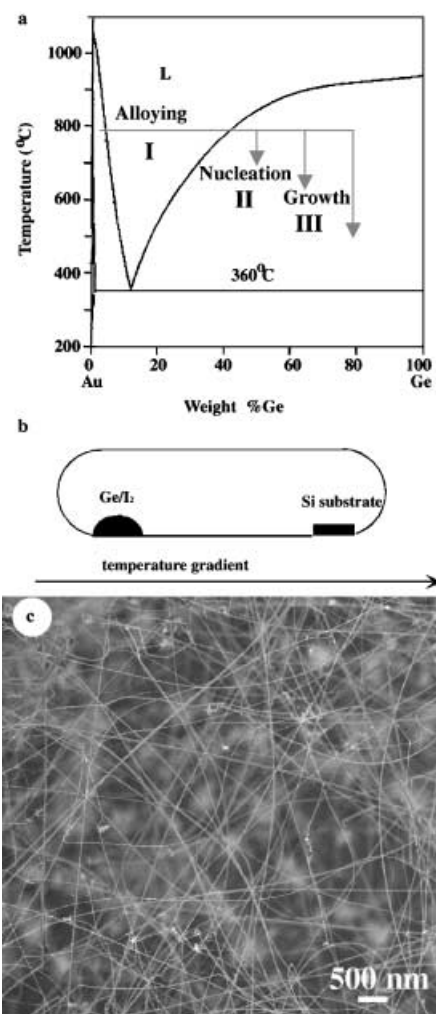


Figure 3. a) Au–Ge binary phase diagram. b) Schematic illustration of the vapor transport tube for the Ge nanowire growth. c) SEM image of the as-made Ge nanowires.

binary phase diagram of the Au–Ge system. As shown in the diagram, Au is a good solvent for the Ge nanowire growth because of the existence of the Au–Ge eutectic. Figure 3b illustrates the chemical vapor transport scheme in a sealed quartz tube. A mixture of Ge/I_2 powder and a Si wafer coated with a thin film of Au are placed at the high- (1000°C) and low-temperature (800°C) end, respectively. Ge reacts with I_2 to form GeI_2 vapor at the hot end, which is then transported to the cold end. GeI_2 then decomposes into Ge and I_2 vapor and forms Ge nanowires as shown in Figure 3c. Nanowires of many different materials have been synthesized by using both chemical and physical methods, including elemental semiconductors (Si and Ge), III–V semiconductors (GaAs, GaP, InP, InAs), II–VI semiconductors (ZnS, ZnSe, CdS, CdSe), and oxides (ZnO, MgO, SiO_2).^[19–26]

The diameter of nanowire is an important parameter. Many physical and thermodynamic properties are diameter dependent. According to the VLS mechanism, the diameter of nanowire is determined by the size of the alloy droplet, which is in turn determined by the original cluster size. By using monodispersed metal nanoclusters, nanowires with a narrow diameter distribution can be synthesized. We have utilized this strategy to grow uniform Si nanowires in a chemical vapor deposition system.^[29] Uniform nanowires with 20.6 ± 3.2 , 24.6 ± 4.0 , 29.3 ± 4.5 , and 60.7 ± 6.2 nm diameters were grown by using Au clusters with sizes of 15.3 ± 2.4 , 20.1 ± 3.1 , 25.6 ± 4.1 , and 52.4 ± 5.3 nm, respectively. Figure 4a shows a field emission scanning electron microscope (FESEM) image of uniform, long and flexible nanowires grown by using 15 nm Au clusters as solvent. Figure 4b shows a TEM picture with both Au clusters and the Si nanowires on the same TEM grid. The correlation between the size of Au clusters and the diameter of Si nanowires can be clearly observed. Similar results have also been observed in GaP nanowires prepared by laser ablation method.^[30]

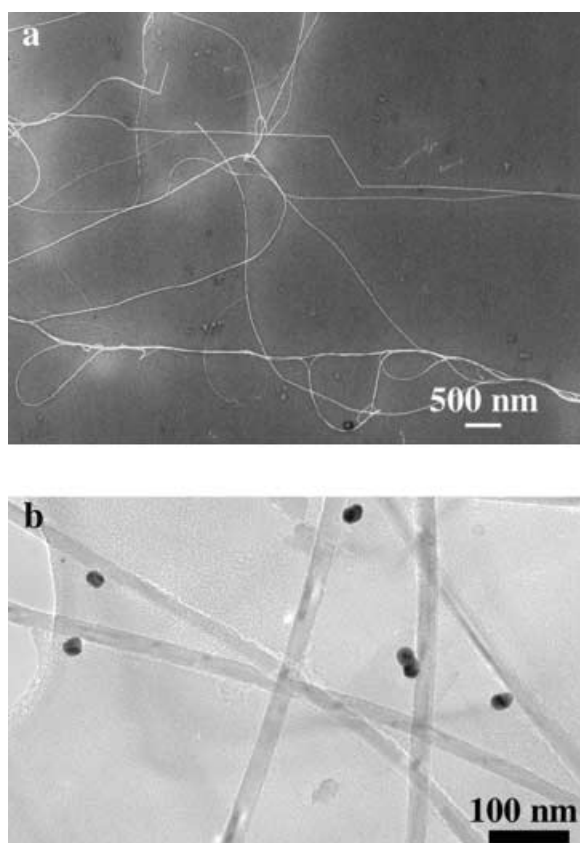


Figure 4. a) FESEM image of Si nanowires grown on Au clusters embedded in mesoporous silica thin film. b) TEM image of the nanowires and the Au clusters dispersed on the same copper grids.

2. Vapor–Liquid–Solid Epitaxial Growth of Semiconductor Nanowire Array

Orientation control: Controlling the growth orientation is important for many of the proposed application of nanowires. By applying the conventional epitaxial crystal growth tech-

nique into this VLS process, it is possible to achieve precise orientation control during the nanowire growth. This technique, vapor-liquid-solid epitaxy (VLSE), is particularly powerful in controlled synthesis of nanowire arrays.

Nanowires generally have preferred growth directions. For example, Si nanowires prefer to grow along the $\langle 111 \rangle$ direction, whereas ZnO nanowires prefer to grow along $\langle 001 \rangle$ direction. One strategy to grow vertically aligned nanowires is to properly select the substrate and to control the reaction conditions, so that the nanowires grow epitaxially on the substrate. Take Si as an example, if a $\langle 111 \rangle$ Si wafer is used as substrate, Si nanowires will grow epitaxially and vertically on the substrate and form a nanowire array (Figure 5a). Figure 5b shows the obtained Si nanowire array grown at 1050°C with SiCl_4 and H_2 as reactants on a $\langle 111 \rangle$ Si wafer. They are typically 80 nm in diameter and 10 microns in length. The effect of epitaxial nanowire growth is evident. If a $\langle 001 \rangle$ Si wafer is used as substrate instead, three sets of oriented Si nanowire arrays can be epitaxially grown out of the wafer surface along the three equivalent $\langle 111 \rangle$ directions

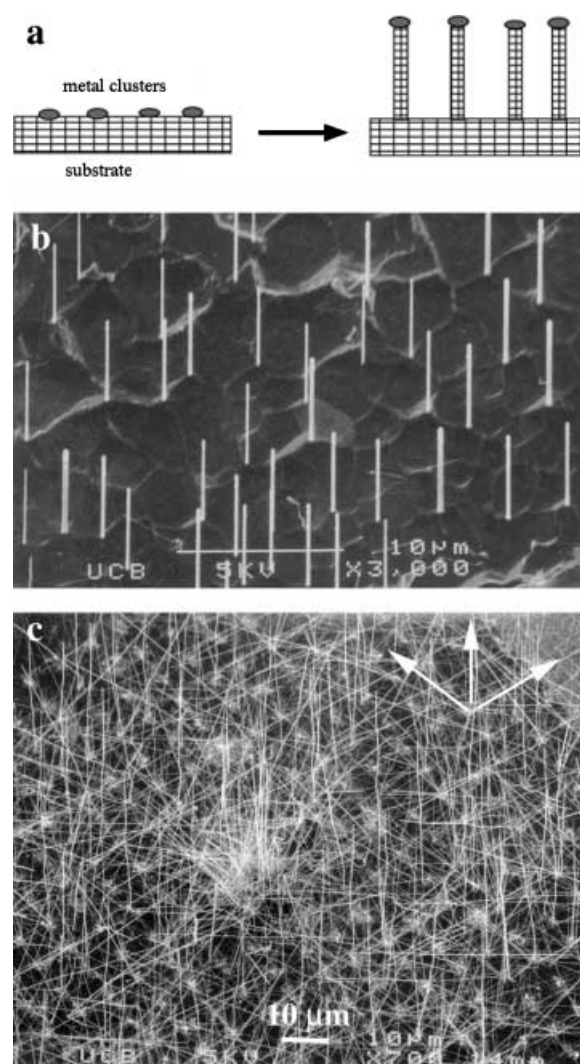


Figure 5. a) Schematic illustration of the VLSE process. b) Vertical Si nanowire array grown on a $\langle 111 \rangle$ Si wafer. c) Three sets of Si nanowire arrays interpenetrate on the surface of a $\langle 100 \rangle$ Si substrate, the three preferred orientations were indicated by arrows.

(Figure 5c). Another VLSE example is the ZnO nanowires grown epitaxially on an *a*-plane (110) sapphire substrate.^[15] ZnO nanowires have wurzite structure with lattice constant $a = 3.24 \text{ \AA}$ and $c = 5.19 \text{ \AA}$ and prefer to grow along the $\langle 001 \rangle$ direction. A ZnO nanowire can grow epitaxially on the (110) plane of sapphire, because the ZnO *a* axis and sapphire *c* axis are related by a factor of four (mismatch less than 0.08% at room temperature, Figure 6a). Figure 6b shows vertical ZnO nanowire arrays grown on the *a*-plane sapphire substrate. Their diameters range from 70–120 nm and lengths can be adjusted between 2–10 microns. Previously, InAs nanowhiskers were oriented on Si substrate by using a fairly complicated metal-organic vapor-phase epitaxy technique.^[31]

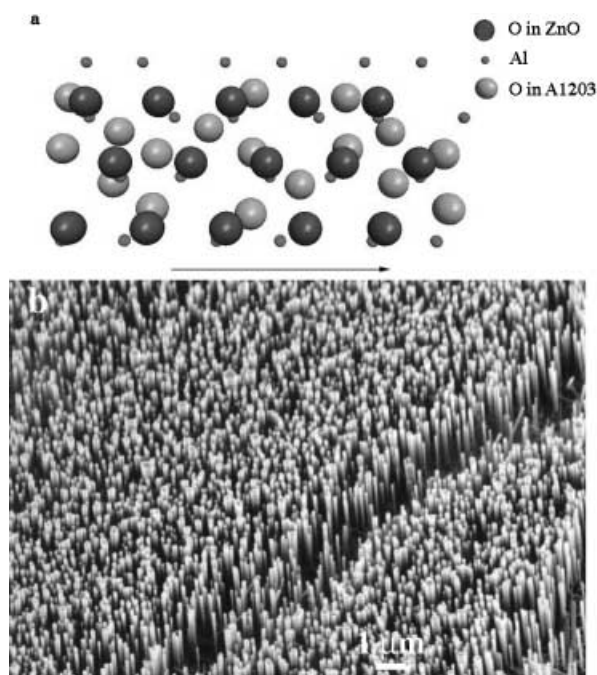


Figure 6. The epitaxial growth of ZnO nanowires on the *a* plane of a (110) sapphire substrate can be readily seen by examination of the crystal structures of ZnO and sapphire ($a = 0.4754 \text{ nm}$, $c = 1.299 \text{ nm}$). a) Schematic illustration of ZnO *ab* plane overlapping with the underlying (110) plane of sapphire substrate. The arrow is drawn along the *a* axis of ZnO structure and the *c* axis of the sapphire crystal structure. b) Arrays of ZnO nanowires grown on the *a* plane sapphire substrate.

Positional control: It is apparent from the VLS nanowire growth mechanism that the positions of nanowires can be controlled by the initial positions of Au clusters or thin films. Various lithographical techniques including, for example, soft lithography, e-beam, and photolithography, can be used to create patterns of the Au thin film for the subsequent semiconductor nanowire growth. Figure 7 shows the SEM images of ZnO nanowires grown from the line and square Au patterns on the *a*-plane sapphire substrate. It is clear that nanowires grow vertically only from the region that is coated with Au and form the designed patterns of ZnO nanowire arrays.^[15]

During the nanowire array growth, generally a thin film of gold was deposited as the solvent/initiator for the nanowire growth. Upon heat-up, these gold thin films will self-aggregate into a high density of Au clusters. The diameters and the

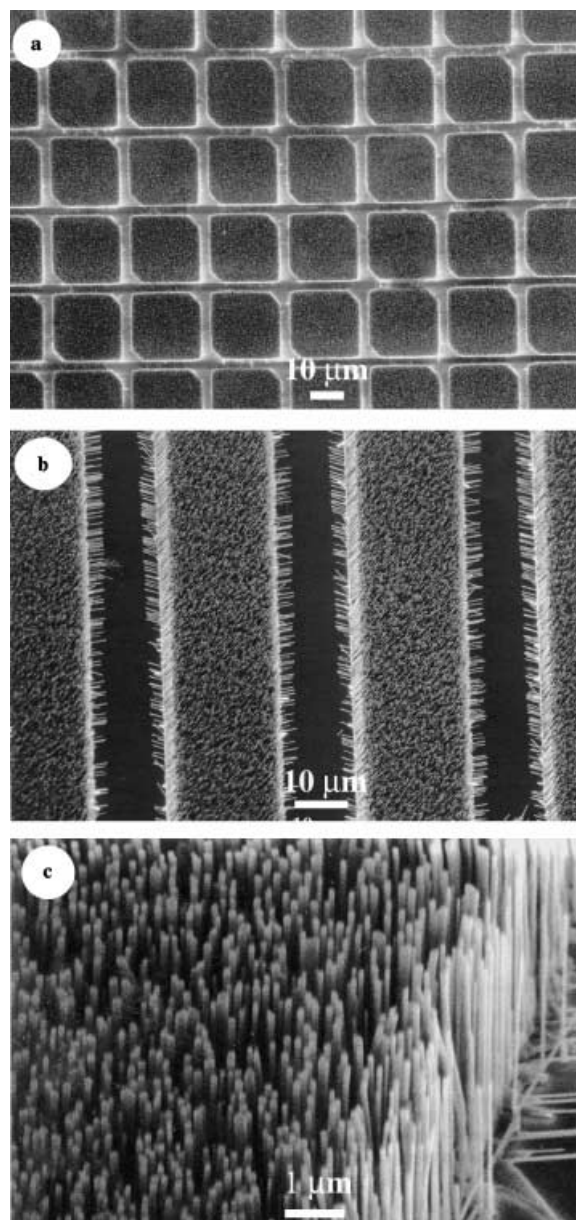


Figure 7. Site-selective growth of ZnO nanowire arrays on *a*-plane substrates. The pattern of nanowire array is defined by the initial Au thin-film pattern fabricated by photolithography.

density of these clusters are determined by the thickness of the thin film and the growth temperature. Thus it is possible to control the nanowire areal density by modifying the thin film thickness. Another approach to control the areal density of the nanowire array is to use the solution-made Au clusters. By dispersing a different amount/density of Au clusters on the sapphire substrate, it is possible to obtain nanowire arrays with different densities. We can now readily synthesize, for example, ZnO nanowire arrays with areal density spanning from 10^6 – 10^{10} cm^{-2} .

Nanowire network growth: As a comparison, when the epitaxial nanowire growth conditions are not satisfied, most of the nanowires will grow parallel to the surface, that is, nanowires “crawl” along the substrate. This surface-parallel

growth is actually important for their potential applications in nanoscale electronics, which requires precise placement of individual wires on substrate with desired configuration. It's critical to have the capability to define the start and end points during the nanowire growth in order to form a surface nanowire network. While the starting point of nanowires can be defined by the positions of metal particles as outlined in the previous section, it's necessary to create certain anisotropic chemical environment so that nanowires can be guided to grow along a preset direction on the substrate surface. A feasible method is to create a local vapor pressure gradient near the nanowire. A nanowire grows faster along the direction with higher vapor pressure. This local vapor pressure gradient can be created by the formation of liquid alloy droplet between the metal solvent (at high temperature) and the nanowire material. Figure 8a shows an SEM image of Si nanowire network growth from patterned Au dots. The Au dots are fabricated by electron beam lithography. Each dot is 300 nm in diameter and 10 nm in thickness. The substrate is an Si (111) wafer. After Si nanowire growth, triangle-shaped

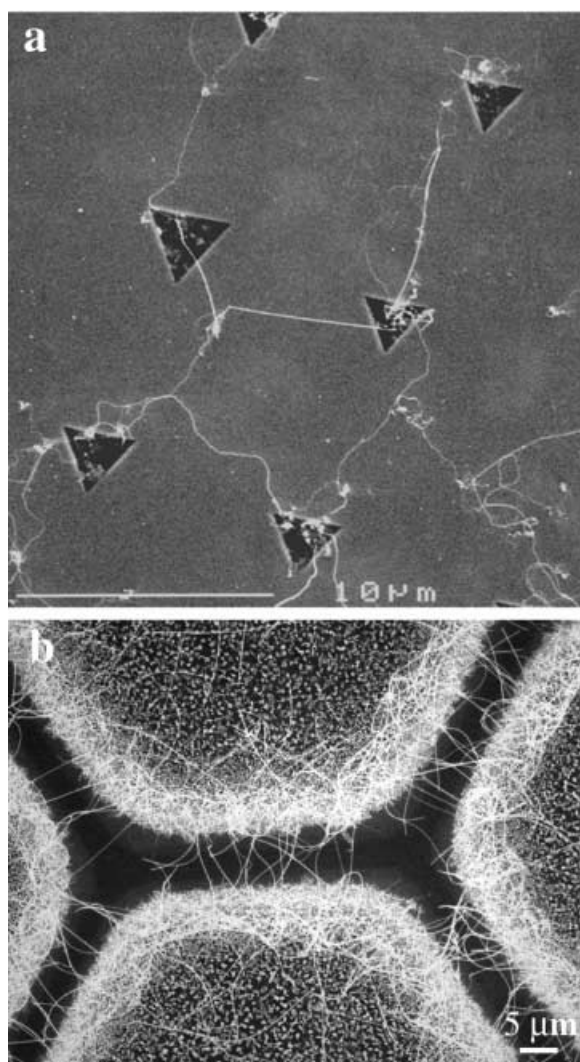


Figure 8. a) Si nanowire network grown on patterned Au dot array. b) ZnO nanowire network grown on Au thin-film hexagonal array. The Au thin-film pattern was generated by shadow mask deposition through a TEM grid.

holes appear at the positions of Au dots as a result of chemical etching. Meantime, Si nanowires grow from one site to the adjacent sites. The liquid alloy phase increases the vapor pressure of Si. As a result, there is a local vapor pressure gradient around each Au dot; this guides the Si nanowire growth from one dot to the adjacent ones. This surface patterning strategy can be readily applied to the ZnO system. Figure 8b reveals extensive growth of fine, long, and flexible ZnO nanowires from the edges of patterned Au hexagons. The wire growth conforms to the hexagonal Au pattern in high fidelity. Most of the wires actually bridge the neighboring metal Au hexagons and form an intricate network.^[20]

3. Thermal Stability of the Semiconductor Nanowires

Compared with bulk materials, low-dimensional nanoscale materials, with their large surface area and possible quantum confinement effect, exhibit distinct electric, optical, chemical, and thermal properties. Thermal stability of the semiconductor nanowires is of critical importance for their potential implementation as building blocks for the nanoscale electronics. A size-dependent melting/recrystallization process of carbon-sheathed semiconductor Ge nanowires has been studied in our laboratory by using an in-situ high-temperature transmission electron microscope.^[32–33]

Ge nanowires with diameters in the range 10–100 nm were made by the VLS mechanism. These nanowires were further coated with a 1–5 nm thick carbon sheath to confine the molten Ge and prevent the formation of liquid droplets at high temperature. Two distinct features are observed during the melting and recrystallization process. One is the significant melting point depression, which is inversely proportional to the radius of nanowire. Another is the large hysteresis during the melting/recrystallization cycle. Figure 9 shows the

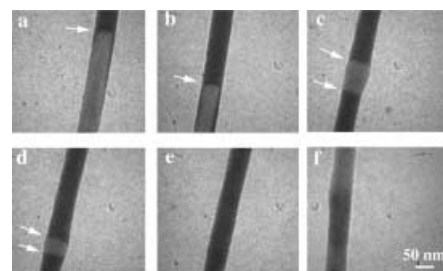


Figure 9. In-situ TEM images of the melting and recrystallization process for a 55 nm Ge nanowire. a) 766 °C, b) 780 °C, c) 842 °C, d) 847 °C, e) 848 °C, f) 558 °C. The solid–liquid interfaces are indicated by arrows.

TEM image sequence during the melting and recrystallization process of a Ge nanowire with a diameter of 55 nm and a length of 1 micron. The melting starts from two ends at around 650 °C (the melting point of bulk Ge is 930 °C) and moves towards the center of the wire as shown in Figure 9a–e. At 848 °C, the whole wire melts. During cooling process, the recrystallization happens at much lower temperature than the initial melting temperature. For this particular nanowire, it

happens at 558 °C as shown in Figure 9f. Significantly, utilizing the low melting points of the nanowires encapsulated in nanotubes, we have been able to manipulate individual nanowires including, for example, in-situ cutting, interconnection, and welding.^[32–33]

The marked reduction in melting temperature for these nanowires in nanotubes has several important implications. First, the optimum annealing temperature for the preparation of high-quality, defect-free nanowires can be expected to be a small fraction of the bulk annealing temperature. It is possible to conduct nanowire zone-refining at a modest temperature with the current simple configuration. Second, the capability of cutting, linking, and welding nanowires at relatively modest temperatures may provide a new approach for integrating these one-dimensional nanostructures into functional devices and circuitry. Finally, as the dimension of the wires is reduced to nanometer length scale, the chemical and thermal stability of the new devices may be limited, which should be considered during the implementation of nanoscale electronics.

4. Semiconductor Nanowire Nanolaser

ZnO is a wide band-gap (3.37 eV) compound semiconductor that is suitable for blue optoelectronic applications, with ultraviolet lasing action being reported in disordered particles and thin films. In addition, ZnO has exciton binding energy as high as 60 meV, significantly larger than that of ZnSe (22 meV) and GaN (25 meV); this indicates that the excitons in ZnO are thermally stable at room temperature. Nanowires of ZnO are thus good candidates as room temperature ultraviolet lasing media.^[15]

The ZnO nanowire arrays were optically pumped by the fourth harmonic of Nd:YAG laser at room temperature to measure the power-dependent emission. Figure 10a shows the evolution of the emission spectra as we increased the pump power. At low excitation intensity, the spectrum consists of a

single broad spontaneous emission peak with a full width at half maximum (FWHM) of approximately 17 nm. This spontaneous emission is generally ascribed to the recombination of excitons through an exciton–exciton collision process in which one of the excitons radiatively recombines to generate a photon. When the excitation intensity exceeds a threshold ($\approx 40 \text{ kW cm}^{-2}$), sharp peaks emerge in the emission spectra. The FWHM line widths of these peaks are less than 0.3 nm, which is more than 50 times smaller than that of the spontaneous emission peak below the threshold. Above the threshold, the integrated emission intensity increases rapidly with the pump power. The narrow line width and the rapid increase of emission intensity indicate that stimulated emission takes place in these nanowires. The fact that we observed lasing action in these nanowire arrays without any fabricated mirror prompts us to consider these single-crystalline, well-faceted nanowires as natural resonance cavities (Figure 10, inset). For our nanowires, one end is the epitaxial interface between the sapphire and ZnO, while the other end is the sharp flat (001) plane of the ZnO nanocrystals. Both can serve as good laser cavity mirrors considering the refractive indexes for sapphire, ZnO, and air are 1.8, 2.45, and 1, respectively. This natural cavity/waveguide formation in nanowires suggests a simple chemical approach to form a nanowire laser cavity without cleavage and etching. This has been further confirmed with the optical characterization of a single ZnO nanowire by near field scanning optical microscopy (NSOM).^[34]

It should be emphasized that the concept of using well-cleaved nanowires as natural optical cavities should be applicable to many other different semiconductor systems such as GaN and CdSe. Our results obtained in ZnO nanowire system suggest the feasibility of nanoscale surface-emitting lasers operating at ultraviolet or other wavelengths when the material of the nanowire cavity is altered. In addition, by creating pn junctions in these individual nanowires, one should be able to test the feasibility of making electron ejection UV/blue lasers out of individual nanowires. Such miniaturized nanowire nanolasers will find applications in nanophotonics and microanalysis.

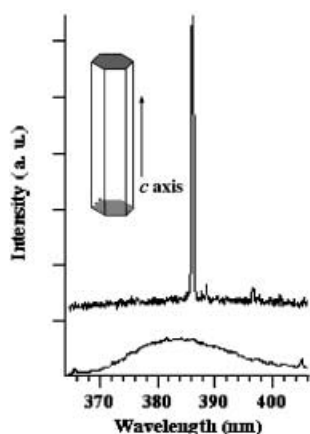


Figure 10. Emission spectra from vertical ZnO nanowire arrays on an *a*-plane sapphire substrate below (bottom trace) and above the lasing threshold (upper trace). The pump powers for these spectra are 20, 150 kW cm^{-2} , respectively. The spectra are offset for easy comparison. The inset shows the schematic illustration of a nanowire as a resonance cavity with two naturally faceted hexagonal end-faces acting as reflecting mirrors.

5. Integration of Nanowires into Functional Networks

The integration of nanowire building blocks into a complex functional structure in a predictable and controlled way represents a major scientific challenge in the nanowire research community. Basically, there are two possible routes. One is to form nanowire superstructures through direct one-step growth process, as illustrated above in the sections of the controlled growth of Si and ZnO nanowire networks and arrays. The other possibility is to develop suitable hierarchical assembly techniques to put nanowire building blocks together into a functional structure. Atomic force microscopes have been used to push or deposit nanotubes into desired configuration.^[17, 35] The shortcoming of this method is that it is slow and time-consuming. We have developed a simple and parallel method in our laboratory dubbed the microfluidic-assisted nanowire integration (MANI) process (Figure 11).^[36]

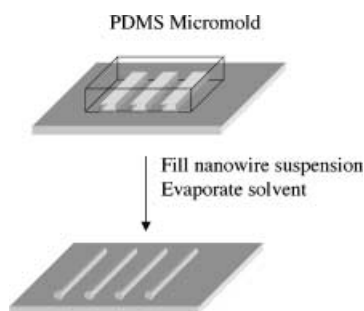


Figure 11. Schematic illustration of the MANI process for nanowire surface patterning.

The microchannels are formed between a poly(dimethylsiloxane) (PDMS) micro mold and a flat Si/glass substrate. The microchannels have a variable height of 1–4 microns, width of 1–10 microns and length of 5–10 mm. This technique has been successfully applied for the alignment of Mo_3Se_3^- molecular wires, conducting polymer nanowires, and carbon nanotubes. Take the Mo_3Se_3^- molecular wires as an example: a droplet of the wire solution/suspension was placed at the open end of the microchannels and the liquid fills the channels under capillary effect. After the evaporation of the solvent and the removal of the PDMS mold, bundles of molecular wires (10–100 nm in diameter) were aligned along the edges of the microchannels and formed parallel array as shown in Figure 12a. After patterning the first layer of nanowires, the process can be repeated to deposit multilayers of nanowires and form complex structures. By rotating the microchannel 90° during the second application, we are able to fabricate

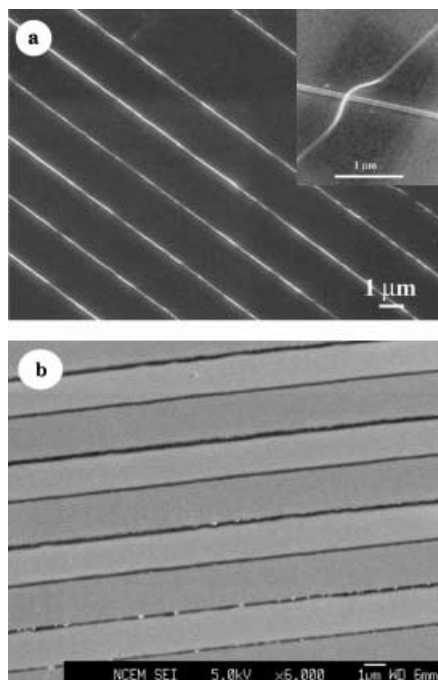


Figure 12. a) SEM image of the aligned Mo_3Se_3^- molecular wire bundles on an Si wafer. The inset shows the cross-junction formed through multiple layer alignment process. A solution of Mo_3Se_3^- molecular wire in methanol was used. b) SEM image of the aligned nanowires of the conducting polymer polyaniline on an Si wafer. Polyaniline aqueous solution was used in the experiment.

arrays of nanowire cross-junctions in a well-controlled and reproducible fashion as shown in Figure 12a, inset. This method provides a general and rational approach for the hierarchical assembly of one-dimensional nanomaterials into well-defined functional networks. Figures 12b and 13 show SEM and atomic force microscope (AFM) images of aligned conducting polymer nanowires and nanotubes on a substrate. The methodology has also recently been extended to the assembly of other inorganic nanowires.^[37]

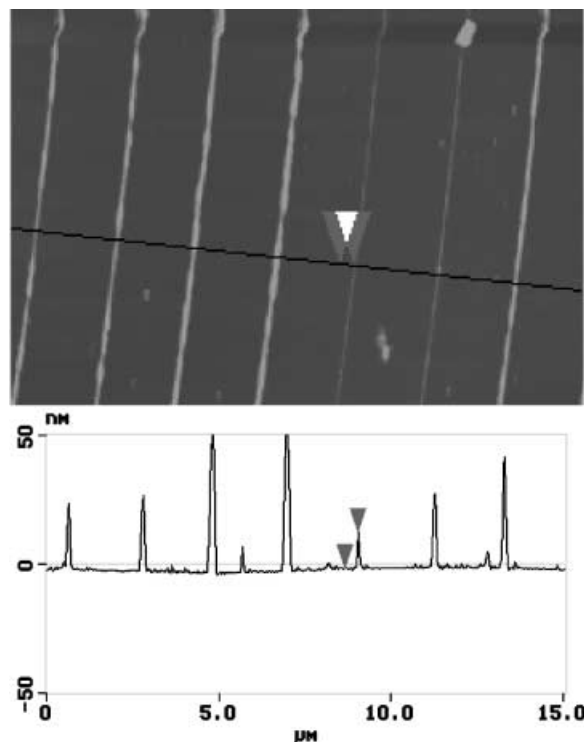


Figure 13. Atomic force microscopy image of aligned carbon nanotube (CNT) bundles on an Si wafer. Sectional height analysis indicates these aligned CNT bundles have diameters in the range 10–60 nm. The CNTs were sonicated in dimethylformamide to form a suspension in the experiment.

Conclusion and Outlook

In this article, we have given a brief survey of work directed toward the rational growth and assembly of semiconductor nanowires. The VLS mechanism has proven to be a valuable guide in choosing metal solvent and reaction conditions. Based on this mechanism, single-crystalline nanowires of a wide range of elemental and compound materials have been prepared. Our capability of growth control represents a significant step toward the applications of nanowires as building blocks in nanoscale electronics and photonics.

The investigation of these one-dimensional nanostructures will continue to be exciting and highly rewarding. Many interesting properties can be investigated, such as electron transport, optical, photoconductivity, thermoelectricity, as well as their chemical properties. With the easy access to many different compositions and possible electronic structures, these non-carbon based inorganic semiconductor nano-

wires surely represent a broad class of nanoscale building blocks for fundamental studies and many technological applications.

Acknowledgement

This work was supported in part by a New Faculty Award from Dreyfus Foundation, a Career Award from the National Science Foundation (DMR-0092086), Department of Energy, and start-up funds from the University of California, Berkeley. P.Y. is an Alfred P. Sloan Research Fellow. P.Y. thanks the 3M company for an untenured faculty award. We thank the National Center for Electron Microscopy for the use of their facilities.

- [1] *Handbook of Nanostructured Materials and Nanotechnology* (Ed.: H. S. Nalwa), Academic Press.
- [2] J. Hu, T. W. Odom, C. M. Lieber, *Acc. Chem. Res.* **1999**, 32, 435.
- [3] *Highly Conducting One-dimensional Solids* (Eds.: J. T. Devreese, R. P. Evrard, V. E. van Doren, Plenum, New York, **1979**.
- [4] E. W. Wang, P. E. Sheehan, C. M. Lieber, *Science* **1997**, 277, 1971.
- [5] L. T. Canham, *Appl. Phys. Lett.* **1990**, 57, 1046.
- [6] J. D. Holmes, K. P. Johnston, R. C. Doty, B. A. Korgel, *Science* **2000**, 287, 1471.
- [7] L. D. Hicks, M. S. Dresselhaus, *Phys. Rev. B* **1996**, 47, 16631.
- [8] Y. Arakawa, H. Sakaki, *Appl. Phys. Lett.* **1982**, 40, 939.
- [9] Y. Arakawa, A. Yariv, *IEEE J. Quantum Electron.* **1986**, 22, 1887.
- [10] Y. Miyamoto, Y. Miyake, M. Asada, Y. Suematsu, *IEEE J. Quantum Electron.* **1989**, 25, 2001.
- [11] Y. Cui, C. M. Lieber, *Science* **2001**, 291, 851.
- [12] T. Rueckes, K. Kim, E. Joselerich, G. Y. Tseng, C. Cheung, C. M. Lieber, *Science* **2000**, 289, 94.
- [13] M. S. Fuhrer, J. Nygard, L. Shih, M. Forero, Y. Yoon, M. S. C. Mazzoni, H. J. Choi, J. Ihm, S. Louie, A. Zettl, P. L. McEuen, *Science* **2000**, 288, 494.
- [14] S. Noda, K. Tomoda, N. Yamamoto, A. Chutinan, *Science* **2000**, 289, 604.
- [15] M. Huang, S. Mao, H. Feick, H. Yan, Y. Wu, H. Kind, E. Weber, R. Russo, P. Yang, *Science* **2001**, 292, 1897.
- [16] *Handbook of Microlithography, Micromachining, and Microfabrication* (Ed.: P. Rai-Choudhury), SPIE Press, IEEE, **1999**.
- [17] C. L. Cheung, J. H. Hafner, T. W. Odom, K. Kim, C. M. Lieber, *Appl. Phys. Lett.* **2000**, 76, 3136.
- [18] R. D. Piner, J. Zhu, F. Xu, S. Hong, C. A. Mirkin, *Science* **1999**, 283, 661.
- [19] Y. Wu, P. Yang, *Chem. Mater.* **2000**, 12, 605.
- [20] M. H. Huang, Y. Wu, H. Feick, E. Webber, P. Yang, *Adv. Mater.* **2000**, 12, 113.
- [21] A. M. Morales, C. M. Lieber, *Science* **1998**, 279, 208.
- [22] C. R. Martin, *Science* **1994**, 266, 1961.
- [23] W. Han, S. Fan, W. Li, Y. Hu, *Science* **1997**, 277, 1287.
- [24] T. J. Trentler, K. M. Hickman, S. C. Geol, A. M. Viano, P. C. Gibbons, W. E. Buhro, *Science* **1995**, 270, 1791.
- [25] Y. Li, Y. Ding, Z. Wang, *Adv. Mater.* **1999**, 11, 847.
- [26] X. Duan, C. M. Lieber, *Adv. Mater.* **2000**, 12, 298.
- [27] R. S. Wagner, W. C. Ellis, *Appl. Phys. Lett.* **1964**, 4, 889.
- [28] R. S. Wagner in *Whisker Technology* (Ed.: A. P. Levitt), Wiley, New York, **1970**, p. 47.
- [29] Y. Wu, P. Yang, *J. Am. Chem. Soc.* **2001**, 123, 3165.
- [30] M. S. Gudiksen, C. M. Lieber, *J. Am. Chem. Soc.* **2000**, 122, 8801.
- [31] S. T. Hiruma, M. Shirai, K. Tominaga, K. Haraguchi, T. Katsuyama, T. Shimada, *Appl. Phys. Lett.* **1995**, 66, 159.
- [32] Y. Wu, P. Yang, *Adv. Mater.* **2001**, 13, 520.
- [33] Y. Wu, P. Yang, *Appl. Phys. Lett.* **2000**, 77, 43.
- [34] J. C. Johnson, H. Yan, R. D. Schaller, L. Haber, R. J. Saykally, P. Yang, *J. Phys. Chem.* **2001**, 105, 11387.
- [35] J. Lefebvre, T. F. Lymch, M. Llaguno, M. Radosavljevic, A. T. Johnson, *Appl. Phys. Lett.* **2000**, 75, 3014.
- [36] B. Messer, J. H. Song, P. Yang, *J. Am. Chem. Soc.* **2000**, 122, 10232.
- [37] Y. Huang, X. Duan, Q. Wei, C. M. Lieber, *Science* **2001**, 291, 630.